Interplanetary shock–induced current sheet disturbances leading to auroral activations: THEMIS observations

Xiaoyan Zhou,[1,2] Xu-Zhi Zhou,[1] Vassilis Angelopoulos,[1] Quanqi Shi,[1,3] Chih-Ping Wang,[1] and Harald Frey[4]

Received 31 October 2012; revised 1 February 2013; accepted 6 February 2013; published 19 June 2013.

[1] We present a unique case of shock-generated tail current sheet (CS) disturbances measured by five THEMIS spacecraft in a tail-aligned configuration from −11 to −17 Re on 3 March 2009 when an interplanetary shock passed by the Earth. The spacecraft were ideally near the tail CS center. The IMF B_z was weakly southward with a 2 h average of −0.4 nT in the shock upstream. At 0602 UT when the shock impinged at the subsolar magnetopause, compressional waves were launched and propagated at a speed of ~2900 km s^{-1} into the tail. Their arrival presented a discontinuity in the magnetic field and plasma density around a THEMIS outer probe. Then, the CS thickness started decreasing and the tail reconnection rate started increasing. About 3–4 min later when the shock in the solar wind compressed the tail magnetopause at the down-tail location of the THEMIS spacecraft, the CS thinning became more significant and abrupt. Consequently, the CS thickness reduced by ~80% from ~16×10^3 to ~3×10^3 km in ~7 min X = −11 Re. At the same time, earthward fast flows and multiple dipolarization fronts were detected in the tail CS and auroral activity similar to a small substorm on the ground. We found that the tail CS and plasma sheet experienced a two-step evolution, which is attributed to the much faster propagation of compressional waves inside the magnetosphere than the shock in the solar wind. During the first step, the local magnetic field and plasma varied with low fluctuations. In the second step, the CS and plasma sheet became very disturbed with fast flows and significant waves presented. Observations also indicated that the magnetotail is not in pressure equilibrium during the shock compression.

Citation: Zhou, X., X.-Z. Zhou, V. Angelopoulos, Q. Shi, C.-P. Wang, and H. Frey (2013), Interplanetary shock–induced current sheet disturbances leading to auroral activations: THEMIS observations, *J. Geophys. Res. Space Physics*, *118*, 3173–3187, doi:10.1002/jgra.50175.

1. Introduction

[2] While there have been few studies of interplanetary shock–generated disturbances in the tail current sheet (CS) [*Miyashita et al*., 2010; *Shi et al*., 2012], there have been numerous studies on whether interplanetary shocks can cause substorms. Using sudden commencements (SCs) as the manifestation of shock impingement on the dayside magnetopause, earlier studies have revealed that the more intense the SCs (indicating more intense interplanetary shocks) are, the more likely substorm expansion phases are to follow [*Schieldge and Siscoe*, 1970; *Kawasaki et al*., 1971; *Kokubun et al*., 1977], and that the IMF B_z in the shock upstream plays an important role in substorm occurrence as well [*Burch*, 1972; *Kokubun et al*., 1977; *Zhou and Tsurutani*, 2001; *Tsurutani and Zhou*, 2003; *Lyons et al*., 2005]. There are also arguments that interplanetary shocks do not trigger substorms [*Liou et al*., 2003] but do induce a negative bay that is not necessarily a substorm. The actual controller is the concurrent IMF B_z at the shock front [*Liou et al*., 2004]. With limited in situ observations in the magnetotail, these previous studies did not treat the magnetotail response per se but rather focused on the correlation between the input (the shock impingement) and the output (AE or AL indices, the ground-based magnetograms, auroral activity, and/or geosynchronous energetic particle injections).

[3] Shock-induced substorms are very similar to isolated substorms in terms of the characteristics of the auroral morphology and variations in the geomagnetic field measured from the ground and from geosynchronous orbit [*Meurant et al*., 2005]. For three events when Geotail was in the tail with no substorms recorded at least 20 min after the corresponding SCs, *Miyashita et al*. [2010] found that

[1]Institute of Geophysics and Planetary Physics, University of California, Los Angeles, California, USA.
[2]On leave from Jet Propulsion Laboratory, California Institute of Technology, Pasadena, California, USA.
[3]Shandong Provincial Key Laboratory of Optical Astronomy and Solar-Terrestrial Environment, School of Space Science and Physics, Shandong University, Weihai, China.
[4]Space Sciences Laboratory, University of California, Berkeley, California, USA.

Corresponding author: X.-Y. Zhou, Institute of Geophysics and Planetary Physics, University of California, Los Angeles, CA 90095, USA. (xyzhou@igpp.ucla.edu)

2169-9380/13/10.1002/jgra.50175

the tail plasma sheet compression was adiabatic, which is not consistent with the non-adiabatic behavior of the substorm-associated plasma sheet. Their explanation was that the magnetotail compression suppressed magnetic reconnection because the observed B_z value in the tail was enhanced. Therefore, substorm expansion onsets were suppressed as well. *Miyashita et al.*'s study raised the question on how the tail plasma sheet evolves during shock-induced substorms or quiescent events.

[4] The magnetotail is a key region for the development and evolution of substorms under all circumstances, including those induced by interplanetary shocks/sudden pressure increases. Moreover, the evolution of the tail CS under solar wind–induced compressions provides further interest to the physics for currents in general and to substorm/storm time magnetotail dynamics in particular. When a shock passes by the tail, the lobe magnetic field strength experiences a step-function-like increase with a certain duration of ~2 to 15 min [*Kawano et al.*, 1992; *Petrinec and Russell*, 1996; *Collier et al.*, 1998; *Tsurutani and Zhou*, 2003; *Kim et al.*, 2004; *Huttunen et al.*, 2005]. On the basis of the pressure balance between the solar wind and the lobe magnetic field and under conservation of the magnetic flux in the tail lobe, an increase in the solar wind dynamic pressure can significantly reduce the lobe size in diameter. Such as for the 24 September 1998 event, the lobe radius at X = −15 Re was reduced by ~30% due to the shock compression [*Zhou and Tsurutani*, 2002].

[5] In addition to the shock compression from the solar wind, there is an internal propagating shock effect, i.e., the compressional waves launched by the shock impingement at the subsolar magnetopause. In the 1960s, it was recognized that these compressional waves propagate inside the magnetosphere at a speed faster than that of the shock propagation in the solar wind [*Dessler*, 1964; *Bame et al.*, 1966; *Patel*, 1968; *Sugiura et al.*, 1968]. The expected propagation speed (at the fast magnetosonic speed) ranges from 200 to 2000 km s^{-1} based on the average tail magnetic field of 10 nT and the tail plasma density of 1 to 0.01 proton cm^{-3} [*Patel*, 1968]. *Brittnacher et al.* [2000] proposed that hydromagnetic waves generated by the pressure pulse impingement on the dayside magnetopause can trigger substorms. Using multipoint observations, *Keika et al.* [2009] identified the front of the compressional waves in the dayside and dawnside magnetospheres and calculated the fast-mode speed to be ~400 to 1600 km s^{-1} with the highest value in the ~0900 to 1500 MLT sector and abruptly reduced to ~400 km s^{-1} toward the near-Earth equatorial magnetotail beyond geosynchronous orbit.

[6] However, neither the relative contribution of the internal compressional waves and the external shock compression nor the effect of the compressions on the CS is well understood. In this paper, we take the unique advantage of the THEMIS mission [*Angelopoulos*, 2008], which provides multiple spacecraft in situ observations with ideal spatial separation along the CS. Furthermore, the mission also provides coordinated observations in the ionosphere, which are crucial for understanding the global consequences of the compressions as well as the coupling of the disturbances measured in situ in the magnetotail to the ionosphere. This paper analyzes a shock event on 3 March 2009 during which five THEMIS probes were near the CS center with a separation of ~7 Re in X from about −10 to −17 Re, ~1 Re in Y, and ~2 Re in Z. During that time, the ground-based THEMIS/ASI network was located near local midnight and provided ASI images for the substorm ionosphere around the footprints of the five probes.

2. Observations in the Tail and on the Ground

2.1. Criteria for Event Selection

[7] Motivated by the desire to understand the evolution of the tail CS and its effects on the ionosphere at times when shocks pass by the Earth, we searched for events during which (1) THEMIS probes were near the CS center but with a separation in X greater than 5 Re, (2) simultaneous observations from the ground ASI were available, and (3) there was no sudden southward or northward turning in the IMF B_z exactly at the shock. In this way, the ambiguity of the tail disturbance triggering can be reduced and the shock effect can be singled out. In the data since THEMIS was launched, we found three shock events with ASI imaging data available. Only one of them fulfills all three criteria. This event occurred on 3 March 2009 with an SC at 0602 UT.

2.2. Solar Wind Observations of the Interplanetary Shock on 3 March 2009

[8] The fast forward interplanetary shock shown in Figure 1 was moderate/weak in intensity with a shock Mach number of ~1.8. The OMNI 1 min solar wind data in the top five panels have been shifted to the subsolar bow shock (http://omniweb.gsfc.nasa.gov/html/HROdocum.html#3). The THEMIS-AL index is shown in the bottom panel. A dashed vertical line marks the shock at which the solar wind dynamic pressure increased from ~1.5 to 4 nPa and then to 5 nPa in the following hour. The solar wind speed was relatively low and increased from 320 to 345 km s^{-1} at the shock. At 2 h in the shock upstream, the IMF B_z was mainly near zero and most of the time between −1 and 0 nT; only on one occasion did it reach 1 nT. The average IMF B_z was −0.4 nT. In the shock downstream, the IMF B_z gradually turned southward and reached −4 nT after 18 min. Later, B_z turned northward to ~5 nT at ~0700 UT.

[9] The THEMIS-AL index in the bottom panel indicates that there were two small intensifications of the westward auroral electrojets measured by the THEMIS ground-based magnetometers before the shock arrival on Earth. The corresponding auroral activity occurred very locally in the field of view (FOV) of the ASI at Rankin Inlet (RANK) (images are not shown in this paper). The increases in the AL magnitude and the auroral activity during 0602–0630 UT are of interest and will be further discussed in the following sections. Note that the shock-related auroral onset also occurred at RANK but was not confined within its FOV.

2.3. Locations of Five THEMIS Probes in the Tail

[10] The locations of the five THEMIS probes and CS sketches are shown in Figure 2, in which the magnetic field lines are traced using the T96 model [*Tsyganenko*, 1996]. The left panels show the locations at 0530 UT before the SC and the right at 0609 UT 7 min after the SC. The corresponding solar wind conditions for the T96 input are given on the top of both columns. In the top row, the CS is

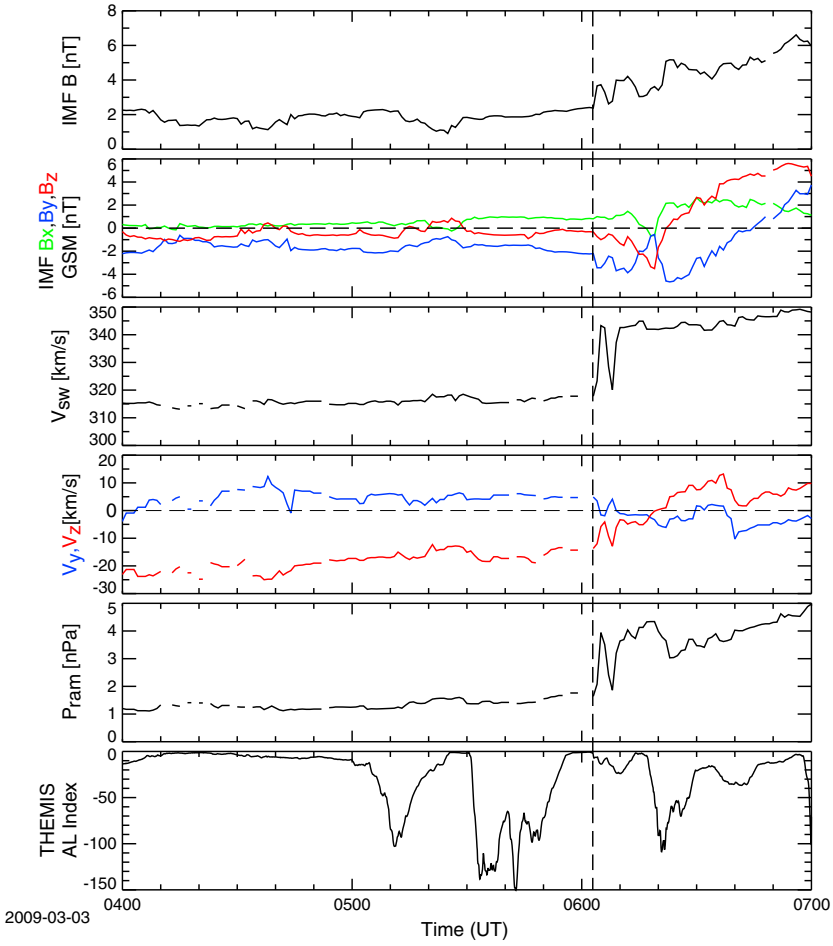

Figure 1. OMNI 1 min solar wind data and the local AL index from the ground-based THEMIS magnetometers on 3 March 2009. The shock is marked by the vertical dashed line. The solar wind data have been shifted to the subsolar bow shock (http://omniweb.gsfc.nasa.gov/html/ HROdocum.html#3).

depicted by a yellow strip. The CS is sketched thinner after the shock compression to depict the thinning inferred from in situ observations in the tail (see the next section). The geomagnetic field near the CS was evidently stretched by the shock-related compression based on the T96 model. The locations of the five probes at 0600 UT are listed in Table 1. Three inner probes, THA, THD, and THE, were at 10–11 Re in the tail with ~1 Re separation in Y and Z, respectively. The two outer probes, THB and THC, at 16–17 Re in the tail were very close in Y and separated by less than 1 Re in Z.

2.4. In Situ Observations From the Outer Probes THB and THC

[11] To distinguish the compression effect generated by the compressional waves inside the magnetosphere as they reached the probes from the compression effect generated by the interplanetary shock in the solar wind as the shock compressing the tail magnetopause right at the corresponding location (along the X axis) of the probes, we will refer to the former effect as the "internal compression" and the latter as the "external compression." The compressional waves launched by the shock impact on the dayside of the magnetopause propagate at a faster speed than the shock in the solar wind. Therefore, the internal compression front arrives ahead of the external compression front; i.e., the THEMIS probes detect the internal compression front and its effects prior to the external compression front and relevant effects.

[12] A further clarification is needed concerning the "arrival." The arrival of the internal compression front represents that of the compressional waves at a THEMIS probe. However, the arrival of the external compression front does not represent the interplanetary shock wave arriving at a THEMIS probe inside the tail CS and/or plasma sheet and instead indicates the arrival of the compression effects generated by the shock when it compresses the magnetopause at the X_{GSM} location corresponding to the probe. These compression effects are significant magnetic field and plasma environment changes resulting from the suddenly reduced lobe diameter as well as the abruptly enhanced current density of the magnetopause current and the cross-tail current due to the external compression. In general, the arrival time can be estimated based on measured magnetic field and plasma variations or calculated based on the solar wind observations, for example, the shock normal and shock speed.

[13] Figure 3 presents the magnetic field and plasma observations of the two outer probes, THB and THC. The

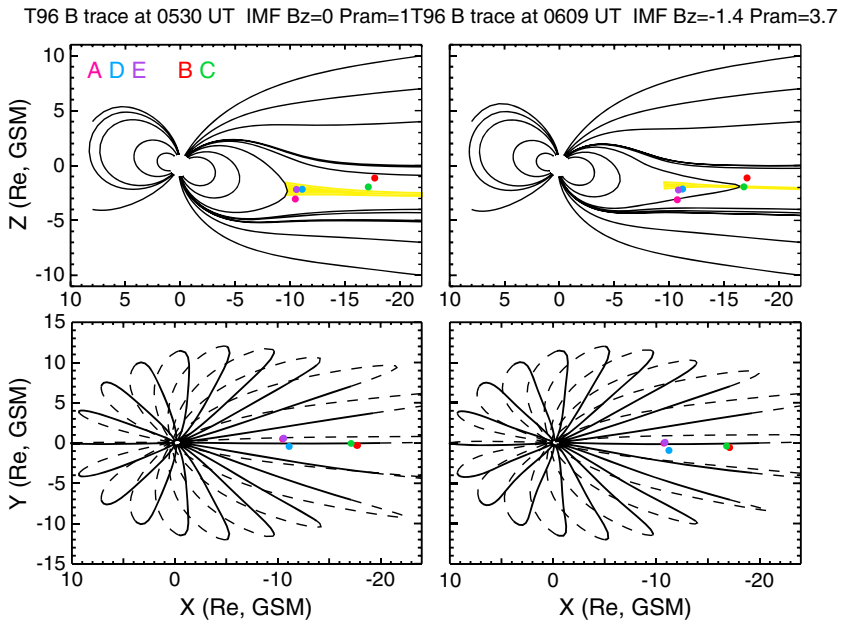

Figure 2. THEMIS locations in the tail before and after the SC time at 0602 UT. The magnetic field trace is from T96.

magnetic data are from THEMIS/FGM (The FluxGate Magnetometer), whereas the plasma data are from THEMIS/ESA (The ElectroStatic Analyzer) and SST (The Solid State Telescope). The colors for each probe are consistent with those in Figure 2. In the top nine panels, the same vector component and parameter from the two different probes are plotted together for comparison. In the bottom two panels, pressure data from the two outer spacecraft are shown in different panels. Thermal pressure (P_{th}) is shown in green, magnetic pressure (P_B, in which the contribution of B_z is excluded) in blue, and total static pressure ($P_{st} = P_{th} + P_B$) in red.

[14] Figure 3 covers a 25 min time duration including a relatively quiet CS and a very disturbed tail CS. Before the shaded area (i.e., before the compression), both outer probes were above the CS center in the outer plasma sheet based on the measured magnetic field strength that was dominated by the B_x component at both probes and the relatively low thermal pressure in the bottom panels. The shaded area at 0603:00–0610:20 UT covers an interval from the beginning to the end of the magnetic field strength increase at THB due to the compression, which is coincidental with the beginning and the end of the total static pressure increase at that probe. The left end of the shaded area at 0603 UT marks the arrival of the internal compression front as shown by a sudden increase in the magnetic field strength and decrease in the plasma density at the probe THB. Note that the sudden increase in the magnetic field was mainly caused by the increase in the B_x component. Such significant effects resulting from the internal compressional waves have not been documented before. Using the SC at 0602 UT as the shock arrival at the nose of the magnetopause (assumed to be 10 Re), the speed of the compressional waves was estimated to be 2900 km s^{-1}, which implies that the internal compression front arrival at the inner probe THA should be at ~0602:40 UT.

[15] After the arrival of the internal compression front at 0603 UT and before ~0607 UT, THC_T_i (the ion temperature at THC) started increasing gradually. Low frequency and low amplitude variations occurred in THC_B_y and THC_B_z (the magnetic B_y and B_z components at THC, respectively) without significant changes in the magnetic field strength. At ~0607 UT (the vertical dashed line), THC_B_x started decreasing abruptly, which resulted in a significant reduction of THC_|B| (the magnetic field strength at THC). At the same time, THC_N_i and THC_T_i started increasing abruptly, indicating a sudden entry into the central plasma sheet. Consequently, the probe encountered a fast earthward flow with a speed of ~200 km s^{-1} (as illustrated in the panel showing V_x). Therefore, we suggest that those sudden enhanced variations with larger amplitude and higher frequency marked the arrival of the external compression front at THC. During the CS crossings at 0607–0610 UT, the B_y component rotated from duskward to dawnward and back to duskward. A dawnward plasma flow accompanied this rotation. The earthward flow continued, intensified, and reached ~500 km s^{-1} at 0613 UT and ~900 km s^{-1} at 0617–0620 UT.

[16] This sudden entry of THC into the CS at ~0607 UT can be attributed to two factors. First, the CS suddenly slowed down the southward motion with a solar wind V_z change from about −15 to −5 km s^{-1} at the shock. This

Table 1. Positions of the Five THEMIS Probes at 0600 UT

Probe	X (Re, GSM)	Y (Re, GSM)	Z (Re, GSM)
A	−10.58	0.15	−3.06
D	−11.21	−0.78	−2.12
E	−10.74	0.31	−2.27
B	−17.25	−0.47	−1.18
C	−16.85	−0.23	−1.96

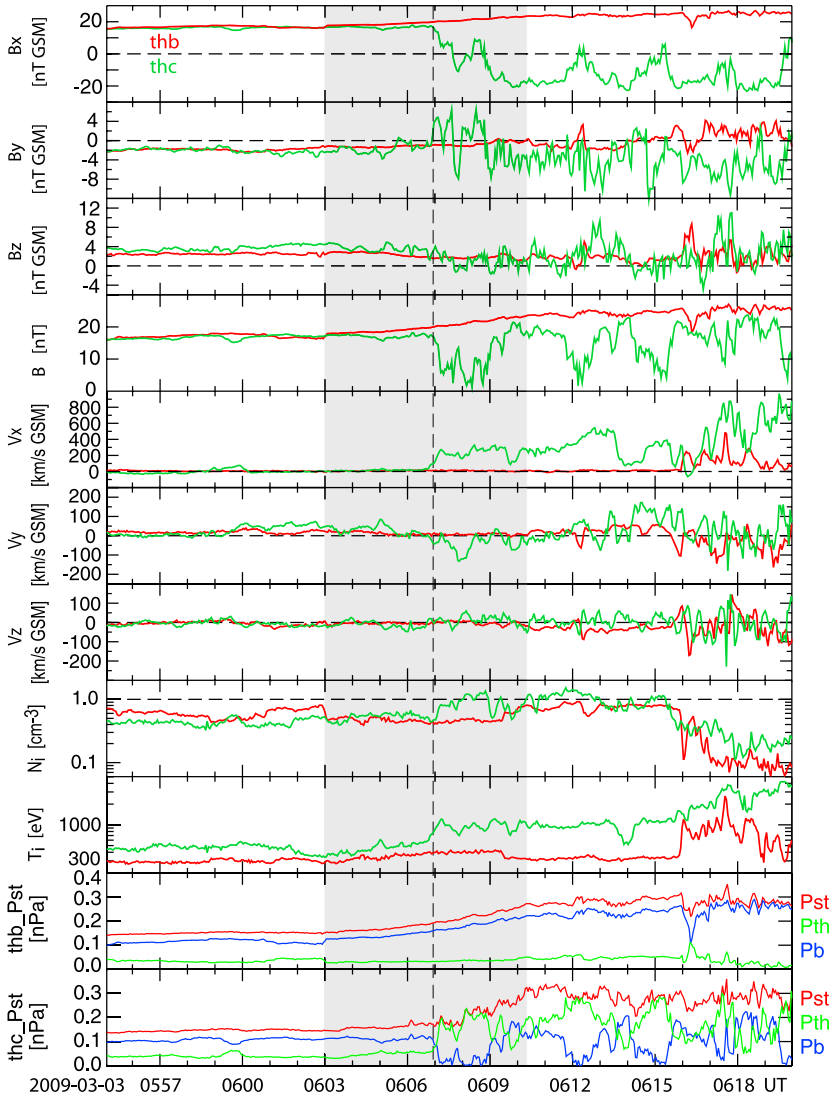

Figure 3. Magnetic field and plasma observations of the two outer probes near X = −17 Re. The colors for each probe are consistent with those in Figure 2. The plasma data are from ESA and calibrated SST. In the top 9 panels, the same vector component and parameter from two different probes are plotted for comparison. In the bottom two panels, pressures from the two outer spacecraft are shown separately in different panels. The thermal pressure (P_{th}) is shown in green, magnetic pressure (P_B, in which the magnetic B_z component is excluded) in blue, and total static pressure ($P_{st} = P_{th} + P_B$) in red. The compression is marked by a shaded area that covers ~0603:00 to 0610:20 UT from the beginning to the end of THB_|B| (the magnetic field strength at THB) increase. The left end of the shaded area is the arrival of the internal compression. The arrival of the external compression front is marked by the dashed vertical line at ~0606:55 UT.

change had the same effect as the CS northward motion that continued after the shock (see Figure 1). Second, with a shock normal of [−0.94, −0.09, 0.33] (in GSM based on Cluster data), the shock may have compressed the southern tail lobe prior to the compression of the northern one. Thus, the CS may have been lifted northward suddenly, which caused the CS entry of THC. Note that while the CS moved northward and THC crossed the CS, the probe THB was not crossing the CS. Instead, the decreasing plasma beta at THB (due to increasing THB_P_B while THB_P_{th} maintained no change in the entire shaded area) indicated THB was relatively moving away from the CS center. These observations implied that the CS thinned due to the compression while THC was entering a thinning CS. Actually, by ~0610 UT, when THB was in the northern plasma sheet boundary layer (PSBL) and THC in the southern PSBL, the CS thickness was less than 5000 km, which is the distance in the Z direction between the two probes. Further discussion about the CS thinning can be found in the next section. The internal and external compressions (marked by the shaded area) increased the total pressure at THB by ~80% and by a factor of ~2 at THC. Before 0603 UT, the P_{st} (as well as P_{th} and P_B) values at the two probes were basically the same at ~1.5 nPa. However, the enhancement of P_{st} at THB after 0603 UT was almost purely by that of P_B, whereas at THC the enhancement was mainly attributed to P_{th} due to the increased N_i and T_i, indicating THC was entering a condensed and hotter CS plasma.

[17] In this section, observations show that the compressional waves propagated down tail to the THEMIS outer probes at a very high speed of ~2900 km s^{-1}. The arrival of the internal compression front presented with a discontinuity in the magnetic field and the plasma density around THB. The plasma sheet measured by THC became very disturbed via a two-step transition initiated by the internal and external compression fronts accordingly. The low frequency and small amplitude variations in the first step were escalated to higher frequency and larger amplitude variations in the second step after the arrival of the external compression front. The CS thinned due to the compressions and the CS thickness was less than 5000 km by 0610 UT.

2.5. In Situ Observations From the Inner Probes THA, THD, and THE

[18] Figure 4 has the same format as Figure 3 and presents magnetic field and plasma observations of the three inner probes. THD and THE were initially at the center of a quiet CS and THA was below the CS center as shown by the panels showing B_x, B, N_i, T_i, and P_{st} from the three probes, respectively. At THD and THE, the magnetic field was mainly in the Z_{GSM} direction. The total pressure P_{st} at the three probes was close to ~0.3 nPa. The shaded interval from 0602:40 to 0609:10 UT marks the beginning and end of the magnetic field strength increase at THA due to the compression, which is coincidental with the beginning and end of the

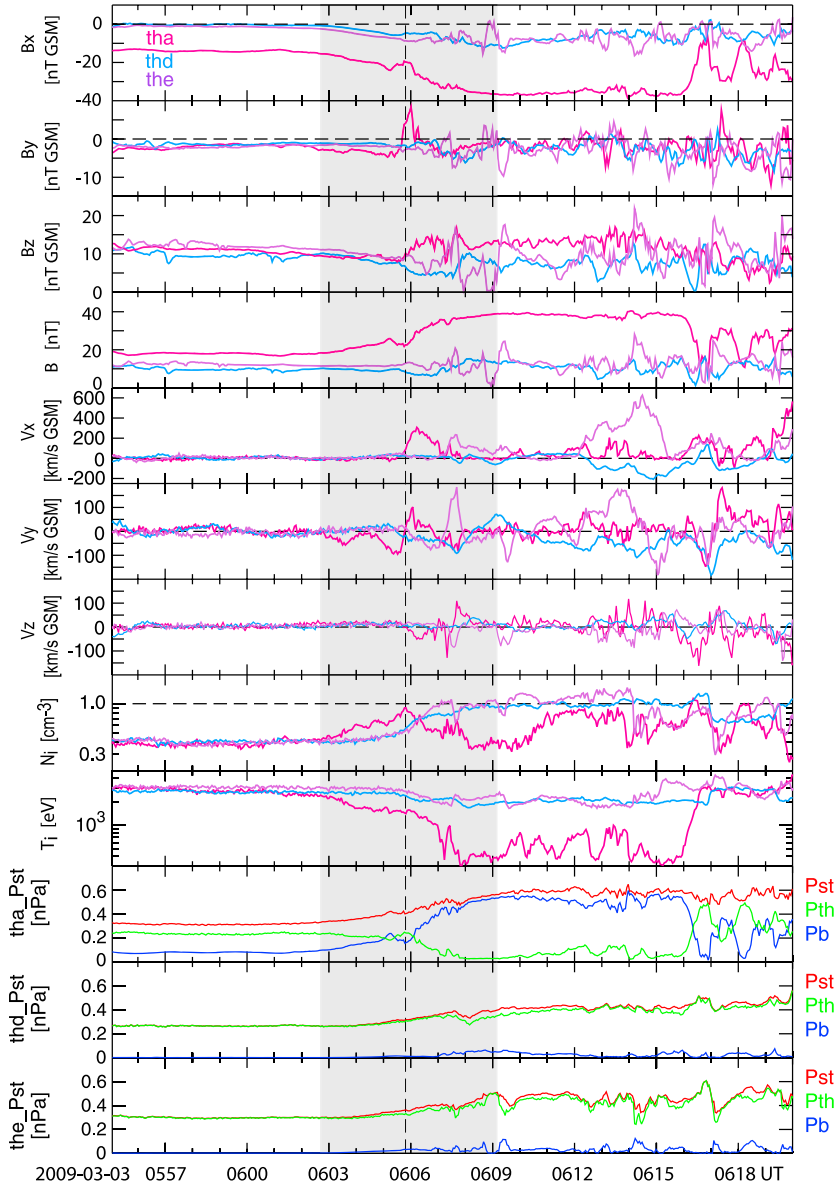

Figure 4. Magnetic field and plasma observations of the three inner probes near X = −11 Re. This figure has the same format as Figure 3. Calibrated SST data are included. A shaded area is marked from ~0602:40 to 0609:10 UT, i.e., the beginning and end of THA_|B| (the magnetic field strength at THA) increase. The left end of the shaded interval marks the arrival of the internal compression. The dashed line at ~0605:45 UT marks the arrival of the external shock compression front.

total static pressure at that probe. The magnetic field strength increase at THA was a factor of ~2. The shaded transition region also appears to be composed by two sections separated by a vertical dashed line. In the first section (to the left of the dashed line), the low frequency variations in the magnetic field and all other plasma parameters were of small amplitude but markedly larger than those prior to 0602:40 UT. In the second section (to the right of the dashed line), such variations were much more intense, especially inside the CS (as evidenced by the data from THD and THE, closest to the CS center).

[19] Since there were no sudden magnetic field strength increases at the inner probes as evidenced by THB, we used the compressional wave speed of 2900 km s^{-1} (inferred from the internal compression front arrival time at the outer probe THB) to determine the arrival time of the internal compression front at THA. The time was around 0602:40 UT (i.e., the left end of the shaded area). From that time, THA_|B| and THA_N_i (the magnetic field strength and ion density at THA, respectively) started increasing gradually, although with decreasing temperature, which we interpret as THA approaching the PSBL from the CS center while the plasma sheet was being compressed by the compressional waves. At the same time, the plasma was moving dawnward. At 0605:45 UT (marked by the vertical dashed line), THA encountered an earthward plasma fast flow of ~300 km s^{-1} (which was mainly in the parallel direction); meanwhile, B_y and V_y suddenly changed from dawnward to duskward, and the B_z component increased to ~6 nT in ~1 min. The ion density turned to an abrupt reduction from a significant enhancement. Furthermore, the magnetic and plasma variations after 0605:45 UT were at higher frequency and larger amplitude compared to those before that time. Therefore, we interpret 0605:45 UT as the arrival time of the external compression front (i.e., the time when THA detected the external compression effects on the internal magnetic field and plasma environment).

[20] The magnetic field strength at THA kept increasing after the arrival of the external compression front and reached ~40 nT at ~0609 UT (the right end of the shaded area). The fact that the increased THA_|B| was mainly attributed to the decreased THA_B_x clearly indicated that the probe was moving further south away from the CS center. At the same time, the temperature and density at THA kept decreasing after 0607 UT and reached the cold and low-density lobe plasma properties at ~0608 to 0609 UT (see the panels showing T_i and N_i). These signatures indicated that THA crossed the PSBL at 0606–0608 UT (see the panel showing THA_P_{th}, when the corresponding beta decreased from 1.00 to 0.06) and may have reached the lobe shortly at 0608–0609 UT (see the very low THA_P_{th} in the same panel; the corresponding beta was well below 1 at ~0.05). With an increasing B field during the compression (in the shaded interval), the magnetic pressure, P_B, enhanced from unremarkable to a dominant component in the total pressure, P_{st}, at the end of the shaded interval. Conversely, P_{th} gradually decreased during that time. The observations are consistent with a motion of THA away from the CS or the motion of the CS away from THA. This relative motion was actually caused by the CS thinning, which will be quantitatively discussed in section 3.2.

[21] From ~0602:40 UT, THD and THE also started moving southward away from the CS center as evidenced by increasing B_x and decreasing B_z magnitudes. The total magnetic field strength remained fairly steady at the two probes until 0605:45 UT (the vertical dashed line). No fast plasma flows were encountered by THD and THE prior to that time. The ion density increased gradually, although the ion temperature remained relatively constant. After the external compression arrival at 0605:45 UT, both THD and THE detected more abrupt variations in N_i and T_i and the variation rate was higher at THE than that at THD (the probe closest to the CS center in the Z direction). Had the three probes been experiencing a CS upward (northward) motion in Z, the density (temperature) at those probes (for all three probes before 0606 UT; for THE and THD after that time) would have increased (decreased) at the same rate (see the panels showing N_i and T_i). Therefore, we conclude that the aforementioned CS upward motion (or the southward motion of the probes) is the manifestation of a CS thinning due to the magnetotail compression by the shock. A quantitative calculation of the CS thickness will be discussed further in section 3.2.

[22] A comparison between data from THA and THE reveals another interesting phenomenon. During the abrupt compression by the external compression front, the high-latitude probe, THA, crossed the PSBL while the low-latitude probe, THE, stayed inside the CS. THE encountered several dipolarization fronts (DFs) at ~0609:20, 0614, 0617, and 0619:30 UT at which N_i suddenly decreased and the B magnitude increased. During the PSBL crossing and/or being in the outer plasma sheet at 0606–0616 UT (see the panel showing T_i), THA encountered several earthward-moving plasma flows, such as those that started at ~0606, 0610:30, and 0613 UT. These flows also had corresponding duskward, duskward, and dawnward components, respectively. Note that the flow beginning times at ~0606, 0610:30, and 0613 UT were 3–4 min ahead of the DFs at ~0609, 0614, and 0617 UT. This timing indicates, according to *Zhou et al.* [2012a, 2012b], that the flows at THA were intrinsically connected with the DFs at THE. On the basis of particle modeling and observation results, *Zhou et al.* [2012a, 2012b] found that the earthward-propagating DF also accelerates and reflects the ambient plasma sheet ions earthward along field lines. As a consequence, the reflected ion stream appears in the PSBL a few minutes prior to DF arrival in the CS. Their particle simulation results also show that such ion flows in the PSBL (also called ion beams) have a crescent-shaped distribution in the velocity space. Whether the earthward flows (started at ~0606, 0610:30, and 0613 UT) had the crescent-shaped distribution ion distribution will be elaborated and shown in the next section.

[23] In this section, we learned that the compressions also caused CS thinning at the inner probes. DFs were detected by THE near the CS center after the arrival of the external compression front. Earthward flows corresponding to the DFs were detected by THA in the PSBL and/or outer plasma sheet, which is consistent with recent modeling and THEMIS observations. The CS and plasma sheet at the inner probes also experienced a two-step evolution from a quiet stage to a very disturbed one. Similarly to the outer probe THC, the two steps were initiated by the internal and external compression fronts, respectively. Variations in the first step were at

low frequency and small amplitude, but those in the second step were at higher frequency and larger amplitude.

2.6. Ion Distributions at the Inner and Outer Probes

[24] Since there was a separation of ~6 Re along the X axis between the inner and outer probes, we can compare the CS and plasma sheet behavior at the inner and middle tails under quiet and compressed conditions and study their correlation. Figure 5 presents a comparison between THE (in purple) and THC (in green) because they were both inside the plasma sheet and/or crossed the CS center after the arrival of the external compression front. In the middle, time series panels have the same format as in Figures 3 and 4. The shaded interval is a superposition of those in

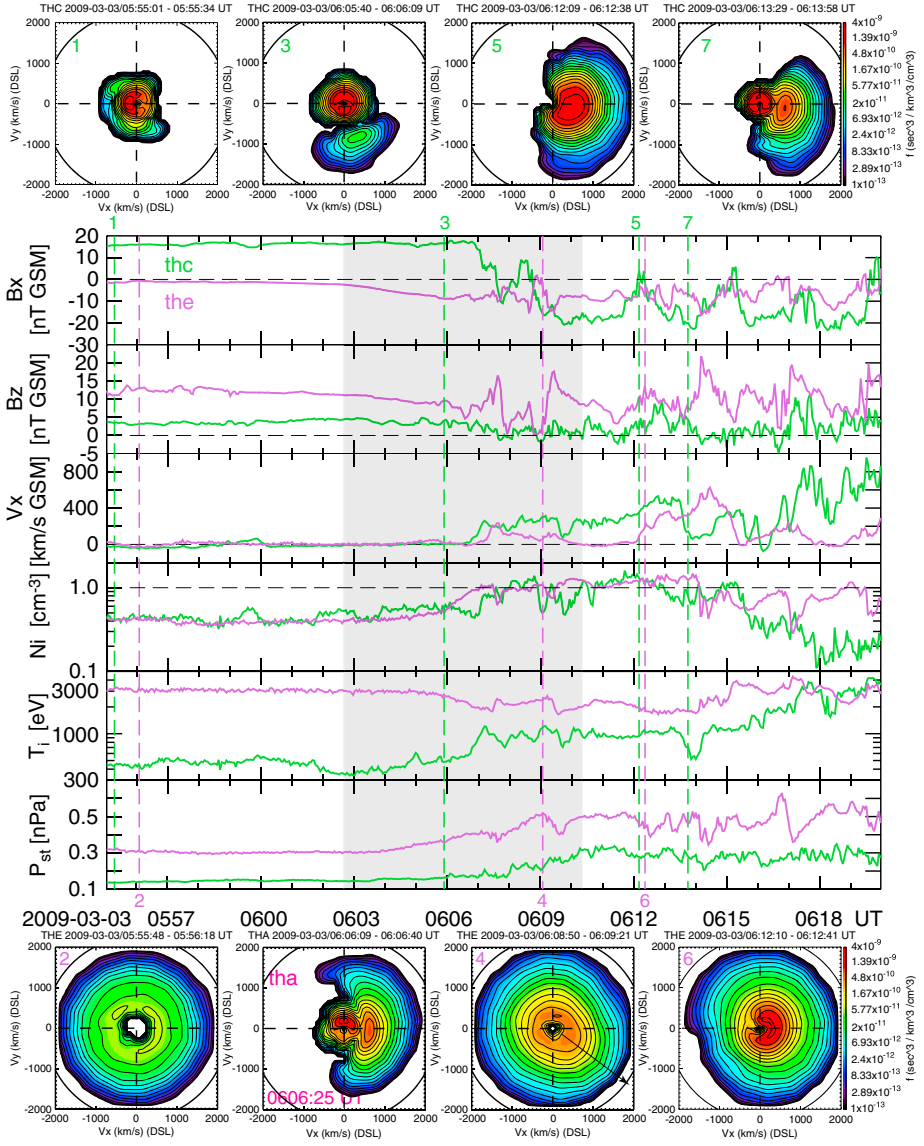

Figure 5. Comparison of ion distributions as well as magnetic and plasma observations between the inner and outer probes THE and THC. The top and bottom rows are 2D ion distributions shown in DSL coordinates. For all velocity slices, the Y axis is V_y (DSL) in −2000 to 2000 km s^{-1} and the X axis is V_x (DSL) in −2000 to 2000 km s^{-1}. Further description of DSL can be found in the text. The color bars have the same scale from 1×10^{-13} to 4×10^{-9} for the phase space density expressed in $s^3/km^3/cm^3$. The top row shows distributions at THC. Each panel is marked by a green digit on the upper left corner corresponding to the time marked by the green digit on the top of the time series plots. At each number, a green dashed vertical line is drawn to show the aligned magnetic field and plasma data. The bottom row is from THE, except the second panel from left, which is from THA. Numbers in purple on the bottom of the time series plots mark the corresponding times of each 2D distribution. In the middle, time series panels have the same format as in Figures 3 and 4. The shading is a superposition of those in the two figures. Ion distributions at time 3 and time 4 plus the one from THA provide a comprehensive picture of the DF at THE, including the reconnection as the cause of the DF tailward of THC and the ion beam (at THA) as the counterpart of the DF in the PSBL.

the two figures. Some of the evident differences in the magnetic field are the large B_z and multiple DFs at THE but smaller B_z and no DF at THC. This may be because THE was close to the CS center, while THC was in the outer plasma sheet most of the time (see the panels showing B_x and B_z). Another explanation can be that the DFs were generated between the two probes, i.e., inside −17 Re. As shown by the V_x component, the earthward plasma flow in the outer plasma sheet at THC was most of the time faster than that near the CS center at THE. Before the compression, the plasma density at both probes was basically the same at ~0.4 to 0.5 cm^{-3}, but the temperature at THE was about 1 order higher than that at THC. From and after 0603 UT (the time of the arrival of the internal compression front), the plasma density increased to ~1 cm^{-3} and abruptly varied due to compression at both locations. At the same time, THE_T_i fluctuated in the range of 2000–5000 eV, while in the outer plasma sheet T_i at THC started and kept increasing gradually. By 0620 UT, THC_T_i increased by about 1 order of magnitude and reached 3000–4000 eV, which was the same as for THE_T_i. The more significant temperature increase at THC than at THE is consistent with the aforementioned comparison of faster plasma flows at THC than at THE, indicating the plasma around the outer probe THC was more abruptly accelerated by the internal and external compressions. The bottom panel shows that, in general, regardless of quiet and compressed conditions, the total static pressure (in the Z direction) at ~11 Re is about a factor of 2 higher than that at ~17 Re in the tail.

[25] Above and below the time series panels, there are 2D ion distributions shown in the despun probe coordinates (i.e., DSL coordinates). Note that the DSL system is roughly along GSE (within 8°) for the inner probes (THA, THE, and THD) and is rotated 180° about the X axis from GSE for the outer probes (THB and THC) due to their southward-pointing spin axes (see *Angelopoulos* [2008] for a detailed description of the coordinate system). For all velocity slices, the Y axis is V_y (DSL) in −2000 to 2000 km s^{-1} and the X axis is V_x (DSL) in −2000 to 2000 km s^{-1}. The background below one count was removed. Each panel has the same color bar scale from 1×10^{-13} to 4×10^{-9} for the phase space density expressed in $s^3/km^3/cm^3$, which is shown on the rightmost ends. The top row shows distributions at THC. Each panel is marked by a green digit on the upper left corner corresponding to the time marked by the green digit on the top of the time series plots. At each number, a green dashed vertical line is drawn to show the corresponding time and to align magnetic field and plasma data. The bottom row is from THE. Numbers in purple on the bottom of the time series plots mark the corresponding times of each 2D distribution.

[26] Before the compression, the tail was relatively quiet at both locations. The ion distribution at time 1 shows that THC was embraced by nearly isotropic and low-temperature plasma in the outer plasma sheet, which is consistent with the magnetic and plasma observations shown and discussed in section 2.4 for Figure 3. Time 2 shows that THE was surrounded by higher-temperature plasma at the center of the CS. At time 3, in addition to the ambient cold population, THC detected a separated ion phase space density peak in the earthward-duskward direction, which, according to *Zhou et al*. [2009], is a remote signature of magnetic reconnection tailward and southward of the probe. This reconnection feature was also detected once by THC at 0602:05 UT (which is before the internal compression arrival at 0603 UT at THC). However, a more frequent occurrence (such as the continuations at 0604:10–0604:30 and at 0605:20–0606:40 UT) indicated that the reconnection rate was evidently increased after the internal compression arrival. At time 4, the ion distribution at the inner probe THE showed a signature of DF, which is a superposition of accelerated ions moving along the earthward-dawnward direction (i.e., the arrow in the bottom panel second to the right) over an otherwise isotropic population. *Zhou et al*. [2012b] pointed out that such distributions are typical in the central plasma sheet right in front of DFs. On the basis of numerous previous reports of the DF and reconnection correlation [e.g., *Sitnov et al*., 2009; *Runov et al*., 2012], it is reasonable to speculate that the DF in the inner tail at time 4 was generated by the reconnections detected earlier at the outer probe THC. Earthward-propagating DF, according to *Zhou et al*. [2012a,2012b], could accelerate and reflect the ambient plasma sheet population earthward and therefore result in field-aligned ion beams with a crescent-shaped ion distribution in the upstream PSBL a few minutes ahead of the DF. These characteristic ion distributions were indeed observed by THA at higher latitudes in the PSBL (see the ion distribution at THA at 0606:25 UT on the bottom and left to the DF ion distribution of THE at time 4). The beginning of such distributions started ~3 min ahead of the DF, which is consistent with the simulation results obtained by *Zhou et al*. [2012b]. The ion distributions at THA at ~0606:25 UT and at THE at time 4 (~0609:05 UT) provided the velocity space description of the first pair of the earthward plasma flow and the DF discussed in section 2.5 for Figure 4.

[27] Time 5 and time 6 were chosen to show the earthward fast flow at the outer and inner probes, respectively, when they were near the CS center. Both centers of the distribution shifted to $+V_x$ in DSL, showing an earthward-directed flow at both locations, while the flow speed (the temperature) at THC was higher (lower) than that at THE. Comparing time 1 to time 2, the plasma temperature difference between THE and THC was clearly reduced. The reduction started from the arrival of the internal compression and was mainly due to the temperature enhancement at THC as discussed above about the panel showing T_i. At time 7, the outer probe THC detected a field-aligned ion beam when it was crossing the PSBL. In addition to the observations depicted in Figures 3 and 4, the ion distributions in Figure 5 also showed stark evidence of shock-induced reconnection, ion beams, and DFs in the disturbed tail plasma sheet and CS.

[28] Observations in this section showed that magnetic reconnection was evidently enhanced by the compressional waves, which occurred on the tail side of the outer probes that were at −17 Re. The reconnection generated multiple DFs that were measured at about −11 Re. The occurrence of the reconnection, ion beams, and DFs at the right time and right location confirmed again that these phenomena are inherently connected and initiated by the same cause. In addition, the shock compression accelerated the plasma in the outer location near −17 Re more efficiently than that near −11 Re.

2.7. Ground-Based ASI Imaging Data

[29] During the shock compression, there were three THEMIS/ASI stations inside the pre-midnight sector with clear sky and there were auroral images available. The stations are, from east to west, RANK, Fort Smith (FSMI), and Inuvik (INUV) that are at 72.4°, 67.4°, and 71.2° MLat, respectively. Images from the three stations are shown in Figure 6, in which midnight is marked by a solid line in each panel. Around the SC time 0602 UT, there was a faint and relatively stable arc at ~72° MLat in the RANK's FOV, which may be the auroral signature of the recovery after a minor auroral activity at ~0530 UT. The arc moved a bit southward and stretched toward midnight by 0606 UT in Figure 6b. A minute later (Figure 6c), a faint auroral arc extended westward to INUV through FSMI. At 0612 UT, in Figure 6d, an auroral breakup was observed by RANK, followed by poleward and westward expansions as shown in Figures 6e to 6h. The aurora reached the maximum latitude of ~74° MLat at ~0624 UT in Figure 6i. Although the auroral intensification in the RANK and FSMI areas ceased, the arc above INUV became sharper and brighter around 0628 UT in Figure 6j.

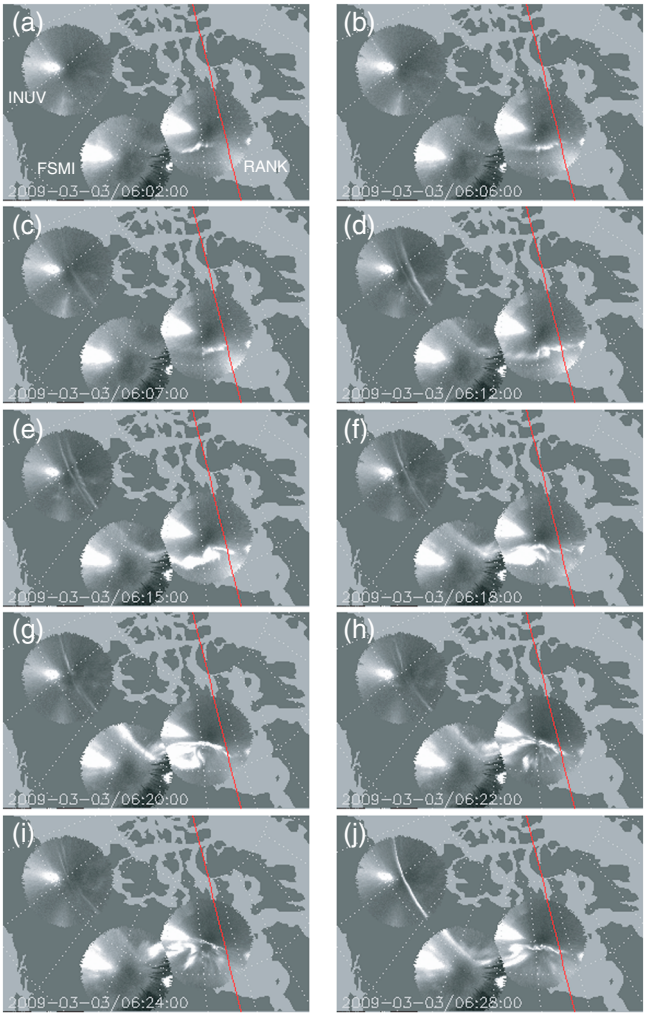

Figure 6. Ground-based auroral imaging data from INUV, FSMI, and RANK at 71.2°, 67.4°, and 72.4° MLat, respectively. Midnight is marked by a solid line in each panel.

[30] During the event, several SuperDARN radars provided good coverage of the polar cap (data not shown here). Radar observations showed that the cap was small and its nightside boundary stayed above 70° MLat, which is consistent with the quiet and stable solar wind condition and the weak westward electrojet (after the shock) shown in Figure 1 as well as with the auroral location. In addition, the auroral evolution in Figure 6 possesses the characteristics of poleward and westward expansions, which are signatures of a classic auroral substorm [*Akasofu*, 1964]. So we would comment that the auroral activity in Figure 6 is similar to substorm auroral activity, although it is a minor one and occurred at high magnetic latitudes.

3. Further Analysis and Discussion

[31] The observations shown and discussed in section 2 have revealed that interplanetary shocks/pressure pulses can generate significant disturbances in the tail CS and plasma sheet, which have not been well documented. Although only one event is presented in this paper, the information from five THEMIS probes and the ground network is very rich and demonstrated the sophistication of the tail CS reaction to a shock/pressure pulse compression. As our first effort, we emphasize the shock effects on the CS and how substorms would be correlated. In addition to the data presented and described in Figures 1–6 and the corresponding text, our current understanding will be elaborated and discussed as follows.

3.1. The Compressional Waves

[32] It is known that the shock impingement on the subsolar magnetopause launches compressional waves into the magnetosphere in all directions [*Dessler*, 1964; *Sugiura et al.*, 1968]. In general, compressional waves propagate inside the magnetosphere faster than the interplanetary shock wave in the solar wind, which means that the effect of the compressional waves should be detected prior to that of the external shock compression on the lobe magnetopause (i.e., the reduction of the lobe radius).

[33] The observations in Figures 3 and 4 show that the internal compression caused the magnetic field strength increase at THB and THA (see the interval at ~0602 to 0606 UT). Consequently, P_B at the two probes increased. Would such enhancements that were purely caused by the internal compressional waves be an implication of the magnetic field strength increase in the entire lobe? Assuming there was no significant magnetic flux added into the lobe from the solar wind with near-zero IMF B_z after a few minutes in the shock upstream, the enhanced lobe magnetic field strength would only be caused by the compressed lobe magnetic flux. Consequently, would the lobe diameter decrease? To address these questions, the pressure equilibrium between the lobe magnetic field and the external solar wind is reviewed in the following. The pressure balance between the solar wind and the tail magnetosphere is described by equation (1):

$$\frac{B_L^2}{2\mu_o} = \left(n_{\mathrm{p}} + n_{\mathrm{He}}\right) V_{\mathrm{SW}}^2 \sin^2\alpha + P_{\mathrm{SW}}^{\mathrm{st}} \tag{1}$$

[34] On the left is the magnetic pressure (we assume that the lobe plasma pressure, or static pressure, is negligible). Here B_L is the magnetic field strength in the tail lobe, but the B_z component is excluded since it does not contribute to the pressure against the magnetopause. On the right, α is the tail flaring angle (the angle between the solar wind flow direction and the tangent to the magnetopause surface) and P_{SW}^{st} is the solar wind static pressure (a sum of the plasma thermal and magnetic pressures). At 1 AU, the solar wind static pressure is about 2 orders lower than the dynamic pressure, so the second term on the right is ignored in this paper. The first term on the right-hand side is the perpendicular component of the solar wind dynamic pressure toward the tail magnetopause [*Fairfield et al*., 1989].

[35] Although both the internal compressional waves and the external solar wind exert pressure on the lobe magnetic field, equation (1) shows that B_L is determined by the external solar wind pressure, as is the lobe radius (i.e., $R_{L2}/R_{L1} = [B_{L1}/B_{L2}]^{1/2}$ assuming the tail magnetic fluxes before (subscript 1) and after (subscript 2) the compression are conserved). The implication, therefore, is that the compressional waves do not increase the total magnetic flux of the lobe. Instead, they redistribute the magnetic field by compressing the field in front of them and leaving a rarefaction region behind them. Consequently, when the magnetic field increased at THB, the magnetic field would have rarefied somewhere else. If this scenario were true, a rarefying magnetic field can be detected after the compressional waves' arrival somewhere in the tail lobe. In other words, the internal compression is more localized, whereas the external solar wind compression is a global (the entire lobe in the Y-Z plane) effect.

[36] The shock-induced magnetic field enhancement in the lobe has been fitted using a step-function-like increase by *Collier et al*. [1998] and *Huttunen et al*. [2005]. This increase has a width ranging from ~2 to ~15 min (varying case by case) instead of a discontinuity like at the shock in the solar wind. In addition to the tension held by the magnetopause and the lobe magnetic field, it was speculated that the large width may be due to a large inclination of the shock normal in the Y direction [*Takeuchi et al*., 2002]. For the 3 March 2009 shock, the width of the magnetic field enhancement (i.e., the shaded areas) was ~7 min. Based on Cluster data, the shock normal was [−0.94, −0.09, 0.33] in GSM and the calculated shock speed was ~380 km s^{-1}. Using the magnetopause location described by *Shue et al*. [1998], we calculated the lobe radius at −17 Re. It was ~23 Re before the SC time of 0602 UT. Thus, the estimated shock passing time through a circle of R = 23 Re in the Y-Z plane is 4.5 min, which is much shorter than 7 min. If using the actual shock speed of ~550 km s^{-1}, which was calculated from the time difference between the two arrivals of the external compression front at the inner and outer probes and their distance of ~6 Re, the shock passing time would be ~3.1 min, which is less than half of the enhancement width of 7 min. The fact that the magnetic field strength enhancement started from the arrival of the internal compression strongly suggests that the large width of the enhancement is due to the internal compressional waves. Therefore, the faster the compressional waves are, the larger the width would be; in addition, the farther down the tail, the longer the width would be. This explains why the shaded interval (i.e., the enhancement width) at the outer location is ~1 min longer than that at the inner location.

3.2. CS Thinning and Magnetic Tension

[37] In sections 2.4 and 2.5, on the basis of in situ observations, we have confirmed that the internal compressional waves caused CS thinning. Since there were multiple spacecraft observations in the CS, we can actually test that conclusion by calculating the CS thickness using the same method as that described by *Zhou et al*. [1997]. As did these authors, we assumed that the magnetic field is anti-symmetric about the CS center and adopted the simple analytical and self-consistent one-dimensional CS model of *Harris* [1962]. In this model, the tail magnetic field and current density are given by

$$B_x = B_L \tanh(z/h) \tag{2}$$

$$j = (B_L/\mu_o h)\,\mathrm{sec}h^2(z/h) \tag{3}$$

where B_L is the lobe field, z is the distance between the spacecraft and the CS center, and h is the half-thickness of the CS. When there are observations from two vertically spaced spacecraft in the CS, h can be derived from equation (2). During the 3 March 2009 shock event, the inner probes THE and THA were less separated in X. So h was calculated by

$$h = 2\Delta z/1n\left[\left(B_L{}^2 + B_L\Delta B_x - B_{xe}B_{xa}\right)/\left(B_L{}^2 - B_L\Delta B_x - B_{xe}B_{xa}\right)\right] \tag{4}$$

where $\Delta z = z_e - z_a$, the distance in Z_{GSM} between THE and THA; $\Delta B_x = B_{xe} - B_{xa}$; and B_{xe} and B_{xa} are the B_x components at THE and THA, respectively. Assuming the lobe magnetic pressure is balanced by the plasma sheet total static pressure, the lobe field is then derived from $B_L = (2\mu_o \mathrm{THA\_P_{st}})^{1/2}$.

[38] The calculated h, the CS center position in Z_{GSM}, and the current density at a few moments are given in Table 2. The calculation shows that before and at the SC time of

Table 2. CS Thickness, CS Center Position, and Current Densities at THA and THE

Time(UT)	B_L[a] (nT)	ΔZ (km)	ΔB_x (nT)	h (10^4 km)	CS Center (Z_{GSM}, 10^4 km)	j_{the} (10^{-9}A/m^2)	j_{tha} (10^{-9}A/m^2)
0555	37.7	5620	10.2	1.60	−1.36	2.00	1.50
0602[b]	37.5	5645	12.5	1.62	−1.33	2.00	1.44
0605	38.7	5655	14.9	1.25	−1.23	2.65	1.45
0607	38.0	5662	22.3	0.60	−1.30	5.51	1.12
0609	38.5	5689	35.2	0.32	−1.40	11.95	0.60

[a]Derived from $\mathrm{THA\_P_{st}}$.
[b]SC time.

0602 UT, h was ~1.6×10^4 km. From 0602 to 0605 UT, h was reduced by ~4000 km, an ~25% reduction, in ~3 min, which was caused by the internal compressional waves. In the following 2 min during which the external compression front arrived, h was reduced more abruptly by ~6500 km. By 0609 UT, after another ~3000 km reduction, h was ~3000 km. So the total shock compression reduced the CS thickness by ~80% in only 6–7 min. From equation (2), the CS center position in Z_{GSM} can be derived and is given in Table 2 in the third column from the right, which shows that the CS position was quite stable through the internal and external compressions. In the two columns from the right, the enhancement of the current density at THE, j_{the}, by the internal compressional waves at 0602–0605 UT was ~33%; however, due to the external shock compression at 0605–0609 UT, j_{the} increased by a factor of ~4.5 from 2.65×10^{-9} A/m^2 at 0605 UT. While not changing during the internal compression, j_{tha} decreased by a factor of 2.4 due to the external shock compression. On the other hand, at 0602 UT and before, the current densities at the two probes were comparable. However, by the end of the shock compression, j_{the} was ~20 times higher than j_{tha}. The contrasting current density variation of the two probes depicts a vivid dynamics of the compressed CS. The results in Table 2 not only quantitatively confirm the CS thinning but also indicate that the external shock compression caused major changes in the CS thickness and the current density in addition to the significant and intense disturbances in the second step discussed in sections 2.4 and 2.5.

[39] In the magnetotail equilibrium theory, the magnetic tension is negligible in the vertical direction along Z [*Birn*, 1987] (i.e., $\partial P_{st}/\partial z = (\mathbf{B}\cdot\nabla)B_z/\mu_o = 0$). Therefore, the total static pressure P_{st} is conserved along Z; i.e., the lobe and CS pressure should balance at all levels of geomagnetic activity [*Baumjohann et al*., 1990]. During the 3 March 2009 event, P_{st} increased at all probes due to the internal and external compressions. However, at the inner probe location, the increase rate was evidently higher at THA than that at THD, with the difference between THA_P_{st} and THD_P_{st} being 0.05 nPa at 0602 UT, 0.11 nPa at 0606 UT, and 0.19 nPa at 0610 UT. This increasing difference implied that $\partial P_{st}/\partial z$ was not close to zero during the compression and that the total static pressure is not constant in the Z direction. The pressure imbalance implies that a magnetic tension was created or significantly enhanced during the compression, so $(\mathbf{B}\cdot\nabla)B_z$ was not negligible. The contribution should be mainly from the B_z variations along the X axis and Z axis around THA, i.e., from $(B_x\partial/\partial x + B_z\partial/\partial z)B_z$. This result indicates that the magnetotail is not in pressure equilibrium during the compression (as shown by the shaded areas in Figures 3 and 4), which is contrary to the assumptions of *Kawano et al*. [1992], *Collier et al*. [1998], and *Huttunen et al*. [2005]. In their studies, only observations in the tail lobe were analyzed.

3.3. Magnetic Reconnection During the Compression

[40] Using test particle simulations under given E and B fields, *Zhou et al*. [2009] showed that the separated peak in ion distributions is a manifestation of the anisotropy resulting from an X-type configuration of the magnetic field. Such features were detected by THC during the 3 March 2009 event (as shown on the top of Figure 5) before the external compression arrival. The reconnection was on the tail side of THC. As described in section 2.6, the occurrence of the reconnection feature significantly increased after the internal compression arrival, which is partially consistent with the MHD simulation by *Hubert et al*. [2006]. Their result predicted that the reconnection rate increases significantly in the compressed magnetotail by interplanetary shocks. But their simulation did not distinguish between the internal and external compressions. The enhanced reconnection was probably the cause of the DFs detected by THE inside the CS at the inner location, which in turn initiated the ion beams detected by THA in the PSBL. The accordant and coincident observations from the five probes confirmed again that the inner tail DFs in the CS and ion beams in the PSBL are inherently connected with the magnetic reconnection in the mid-tail region.

[41] A few minutes after the enhanced reconnection, a thin auroral arc emerged from 0607 UT along the west-east direction across the sky from RANK to INUV covering ~4 h in local time (as shown in Figure 6c). We interpret the elongated west-east auroral arc as an ionospheric manifestation of the CS thinning as a whole in the Y direction due to the internal compression. Then, an auroral breakup occurred at ~0612 UT at RANK (Figure 6d). In addition to the latitudinal expansion of the breakup aurora, it also expanded westward along the existing west-east arc. The auroral breakup and evolution coincided with the suddenly enhanced CS thinning and disturbances in the tail. Especially, the CS thinning provided a condition with the potential for instabilities in addition to magnetic reconnection, which are important triggers for substorm onset.

3.4. Big Picture View of the Shock and Magnetotail Interaction

[42] *Zhou and Tsurutani* [2002] proposed a "dripping, tilting bucket" model to depict the shock and magnetotail interaction and its possible effects on the ionosphere. In this model, as shown in Figure 7, the bucket presents the magnetotail, an energy reservoir into which the solar wind energy is input via the dayside magnetic reconnection. The energy is constantly dripping and leaking from small holes (representing the plasma drafting, convection, and distant tail releasing), which balance the quiet time solar wind energy input.

[43] The left column shows the energy input and storage corresponding to three IMF B_z conditions, and the right column shows the shock effect that initiates and/or facilitates the sudden energy release, which is analogous to a sudden tilt of the bucket. For simplicity, the shock intensity is the same (i.e., same title angle) for the three IMF B_z conditions. When there is a long-duration and large southward IMF B_z, the greatest rate of energy input occurs. The energy storage is near or above the threshold of the reservoir capacity. Substorms happen along with the strong plasma convection to the dayside magnetosphere and the plasmoid released to the distant tail (leakages from small holes in the top left panel). The shock compression elevates the energy release and intensifies the ongoing substorm activity (top right). When the averaged B_z is ~0 in ~1.5 h shock upstream solar wind, the dayside reconnection weakens. While there may still be energy input into the tail reservoir, the storage level is a bit below the capacity threshold. There was no substorm

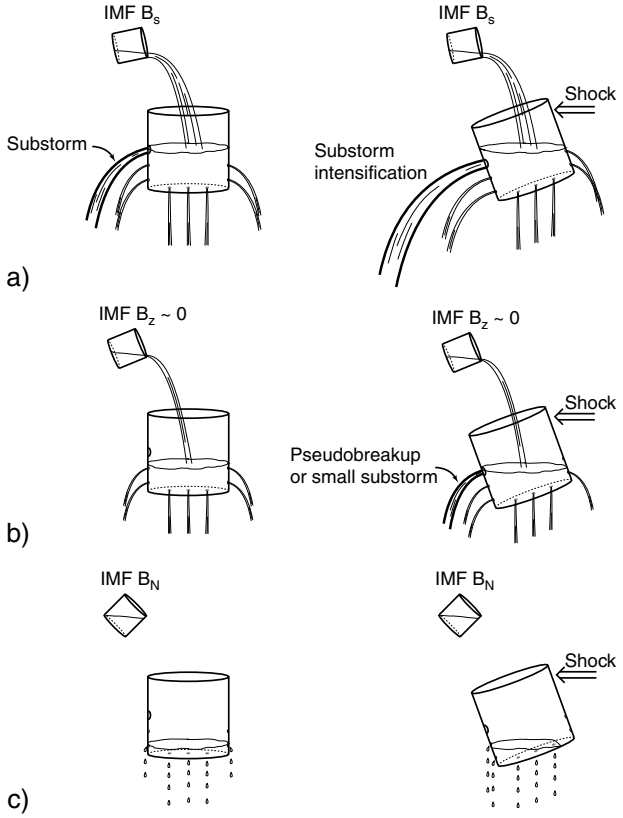

Figure 7. A depiction of the dripping, tilting bucket model (adapted from *Zhou and Tsurutani* [2002]). Panels (a) to (c) describe three IMF preconditions in the shock upstream solar wind of southward IMF (IMF B_S), neutral IMF (IMF $B_Z \sim 0$), and northward IMF (IMF B_N), respectively. On the right of Figure 7b, in addition to pseudobreakups and small substorms, other minor auroral ionospheric activities may also be possible, such as weak westward electrojets, high-latitude substorms, and PBIs along the nightside auroral oval, among others.

activity, but steady magnetospheric convection may have been in progress (middle left). The shock compression triggers instabilities that may lower the threshold level, which is analogous to a tilted bucket leading to a sudden release of the available, but small amount of, energy. A pseudobreakup or small substorm or poleward boundary intensification (PBI) along the auroral oval may occur (middle right). When there is a strong and long-duration northward IMF, the energy input via dayside reconnection stagnates. The energy storage becomes much lower than the threshold, and the plasma convection and energy leaking slow down (bottom left). The shock compression may create some disturbances in the tail. But by tilting a nearly empty bucket, the shock compression cannot cause a sudden energy release that is necessary for even a small substorm (bottom right).

[44] In reality, the shock intensity varies and the IMF B_z precondition differs from case to case. Therefore, the combination of the two components can be more complicated. But the principle of the model is still valid. In general, for the similar shock intensity (as described in Figure 7), the IMF precondition determines whether a substorm happens and whether it is a major or minor one [*Zhou and Tsurutani*, 2001; *Meurant et al*., 2005]. On the other hand, for the similar IMF precondition, the shock intensity determines the amount of the energy release (i.e., whether a substorm is to occur or to be further intensified) [*Kawasaki et al*., 1971; *Burch*, 1972]. In this model, we assumed that the shock only facilitates the release of preexisting energy in the reservoir but does not add significant amount of energy into the reservoir within a short compression duration of ~10 min.

[45] The 3 March 2009 event is similar to the combination shown by the middle right panel in Figure 7. Before the shock arrival, two weak electrojets at ~0505 and 0530 UT had reduced the energy storage in the tail reservoir. However, the shock compression, which is analogous to a tilting of the bucket, caused significant CS disturbances that can be detailed as abrupt CS thinning, magnetic reconnections, fast earthward flows, and DFs. Consequently, a weak auroral activity similar to a substorm was triggered. Another example is the three tail events studied by *Miyashita et al*. [2010]. The event on 8 January 1998 has a strong and long-lasting northward IMF B_z precondition (5–12 nT for more than 6 h in the shock upstream). The magnetic flux and solar wind energy input into the tail were at the lowest level, and, consequently, there was no sufficient energy to be released by the shock compression/tilting as shown in Figure 7c. Geotail at [−28, −0.1, −3 Re] GSM did not detect enhanced CS and plasma sheet disturbance, and no substorm activity was recorded from the ground either.

4. Summary and Conclusions

[46] The uniqueness of shock events includes that two compression processes are generated in the magnetotial during one shock passage. One is the internal compression caused by the compressional waves launched by the shock impact. The wave propagates into the magnetosphere/magnetotail at the magnetosonic speed. The other is the external compression by the shocked solar wind on the magnetopause. This external compression generates intense internal effects, including abrupt CS thinning, abrupt magnetic field strength increase, and/or CS disturbances. The current densities of the magnetopause current and cross-tail current increase abruptly as well. This external compression and its internal effects move tailward with the interplanetary shock at the solar wind speed. Observations also indicate that the magnetotail is not in pressure equilibrium during shock compression, which is contrary to the equilibrium assumption used in previous studies.

[47] In this paper, we have elaborated CS disturbances generated by a fast forward interplanetary shock of moderate/weak intensity (with a Mach number of 1.8) in a relatively quiet solar wind background. For this particular event, the compressional waves propagated at ~2900 km s^{-1} inside the magnetosphere and the shock propagated at ~550 km s^{-1} in the solar wind. There was clear evidence in the data that the tail CS and plasma sheet experienced the two compression processes. Accordingly, a transition occurred in two steps: During the first step, which was initiated by the arrival of the compressional wave front, the local magnetic field and plasma varied with low fluctuations. The first step started ~3 min earlier than the second step at the inner probe location and ~4 min earlier at the outer location. In the second step, which was initiated by the arrival of the external compression front, the CS and plasma sheet became very

disturbed with fast flows and significant waves present. This two-step evolution transformed the tail CS and plasma from quiescence into a striking contrast of disturbance.

[48] The advantage of the five THEMIS probes ideally located at the CS center and outer plasma sheet in the inner and middle tails allowed us to identify the two compression processes and corresponding effects and to understand what the disturbances were and how they were related. We found that the shock caused significant CS thinning at an average rate of ~2000 km/min, which reduced ~80% of the CS thickness from ~16×10^3 to ~3×10^3 km in ~7 min. Note that ~30% of the CS thickness reduction was caused by the internal compression of the compressional waves within 3 min before the external compression front arrived. Such an important effect has not been documented before. This shock also caused an enhancement of the magnetic reconnection tailward of THC. In addition, earthward fast flows and DFs in the CS, ion beams in the PSBL, density and temperature fluctuations, and enhanced wave activity were significant as well. We comment that while the compressional waves do not change the total magnetic flux inside the lobe magnetopause, they redistribute the flux density.

[49] The shock generated a small auroral substorm in the ionosphere, which confirmed previous studies about the effects of interplanetary shocks on the ionosphere. This event showed again that those effects are a combination of the shock intensity and upstream IMF conditions. We found that the substorm initiation is consistent with the passage of the shock (not the internal compressional waves), i.e., when the external compression effects are the most intense.

[50] We have described the auroral signature shown in Figure 6 as a weak westward electrojet or a weak auroral activity similar to a substorm based on the auroral poleward and westward expansions and the occurrence of magnetic reconnection and DFs in the tail CS. We note that such phenomena may also be described as a high-latitude substorm [*Loomer and Gupta*, 1980], a pseudobreakup [*Akasofu*, 1964], or a PBI [*de la Beaujardière et al*., 1994], depending on one's perspective on the phenomena. The main contribution of this study is the shock-generated CS and plasma sheet disturbances and their possible effects on the auroral activation. We would like to leave the readers with some space for the phenomenological interpretation of the auroral signature.

[51] **Acknowledgments.** This study was funded by NASA THEMIS contract NASA-02099. Quanqi Shi was supported by NNSFC award 41031065. We thank J.W. Bonnell and F.S. Mozer for use of EFI data; D. Larson and R.P. Lin for use of SST data; C.W. Carlson and J.P. McFadden for use of ESA data; K.H. Glassmeier, U. Auster, and W. Baumjohann for use of FGM data provided under the lead of the Technical University of Braunschweig and with financial support through the German Ministry for Economy and Technology and the German Center for Aviation and Space (DLR) under contract 50 OC 030; and S. Mende and E. Donovan for use of the ASI data. We acknowledge CSA and NSF award 1004736 for data retrieval, archiving, and processing from the THEMIS GBO stations. We also acknowledge use of the NASA/GSFC Space Physics Data Facility's OMNIWeb (or CDAWeb or ftp) service and OMNI data.

References

Akasofu, S.-I. (1964), The development of the auroral substorm, *Planet. Space Sci.*, *12*, 273.

Angelopoulos, V. (2008), The THEMIS mission, *Space Sci. Rev.*, *141*, 5–34, doi:10.1007/s11214-008-9336-1.

Bame, S. R., J. R. Asbridge, H. E. Felthauser, R. A. Olson, and I. B. Strong (1966), Electrons in the plasma sheet of the earth's magnetic tail, *Phys. Rev. Lett.*, *16*, 138.

Baumjohann, W., G. Paschmann, and H. Lühr (1990), Pressure balance between lobe and plasma sheet, *Geophys. Res. Lett.*, *17*, 45–48, doi:10.1029/GL017i001p00045.

Birn, J. (1987), Magnetotail equilibrium theory: The general three-dimensional solution, *J. Geophys. Res.*, *92*, 11,101–11,108.

Brittnacher, M., M. Wilber, M. Fillingim, D. Chua, G. Parks, J. Spann, and G. Germany (2000), Global auroral response to a solar wind pressure pulse, *Adv. Space Res.*, *25*(7/8), 1377–85.

Burch, J. L. (1972), Preconditions for the triggering of polar magnetic substorms by storm sudden commencements, *J. Geophys. Res.*, *77*, 5629–5632, doi:10.1029/JA077i028p05629.

Collier, M. R., J. A. Slavin, R. P. Lepping, K. Ogilvie, A. Szabo, H. Laakso, and S. Taguchi (1998), Multispacecraft observations of sudden impulses in the magnetotail caused by solar wind pressure discontinuities: Wind and IMP8, *J. Geophys. Res.*, *103*, 17,293–17,305, doi:10.1029/97JA02870.

Dessler, A. J. (1964), Length of magnetospheric tail, *J. Geophys. Res.*, *69*, 3913.

de la Beaujardière, O., L. R. Lyons, J. M. Ruohoniemi, E. Friis-Christensen, C. Danielsen, F. J. Rich, and P. T. Newell (1994), Quiet time intensifications along the poleward auroral boundary near midnight, *J. Geophys. Res.*, *99*, 287–298, doi:10.1029/93JA01947.

Fairfield, D. H., et al. (1989), Substorms, plasmoids, flux ropes, and magnetotail flux loss on March 25 1983: CDAW 8, *J. Geophys. Res.*, *94*, 15135.

Harris, E. G. (1962), On a plasmas heaths eparatinrge gionso f oppositely directedm agneticf ield, Nuovo CirnentoX, Xiii, 115.

Hubert, B., M. Palmroth, T. V. Laitinen, P. Janhunen, S. E. Milan, A. Grocott, S. W. H. Cowley, T. Pulkkinen, and J. C. Ge´rard (2006), Compression of the Earth's magnetotail by interplanetary shocks directly drives transient magnetic flux closure, *Geophys. Res. Lett.*, *33*, L10105, doi:10.1029/2006GL026008.

Huttunen, K. E. J., J. Slavin, M. Collier, H. E. J. Koskinen, A. Szabo, E. Tanskanen, A. Balogh, E. Lucek, and H. R. Re`me (2005), Cluster observations of sudden impulses in the magnetotail caused by interplanetary shocks and pressure increases, *Ann. Geophys.*, *23*, 609–624.

Kawano, H., T. Yamamoto, S. Kokubun, and R. P. Lepping (1992), Rotational polarities of sudden impulses in the magnetotail lobe, *J. Geophys. Res.*, *97*, 17,177–17,182, doi:10.1029/92JA01250.

Kawasaki, K., S.-I. Akasofu, F. Yasuhara, and C.-I. Meng (1971), Storm sudden commencements and polar magnetic substorms, *J. Geophys. Res.*, *76*, 6781.

Keika, K., and R. Nakamura (2009), Substorm expansion triggered by a sudden impulse front propagating from the dayside magnetopause, *J. Geophys. Res.*, *114*, A00C24, 12, doi:10.1029/2008JA013445.

Kim, K. H., C. A. Cattell, D. H. Lee, A. Balogh, E. Lucek, M. Andre, Y. Khotyaintsev, and H. Rème (2004), Cluster observations in the magnetotail during sudden and quasiperiodic solar wind variations, *J. Geophys. Res.*, *109*, A04219, doi:10.1029/2003JA010328.

Kokubun, S., R. L. McPherron, and C. T. Russell (1977), Triggering of substorms by solar wind discontinuities, *J. Geophys. Res.*, *82*, 74–86, doi:10.1029/JA082i001p00074.

Liou, K., P. T. Newell, C. I. Meng, C. C. Wu, and R. P. Lepping (2003), Investigation of external triggering of substorms with Polar ultraviolet imager observations, *J. Geophys. Res.*, *108*(A10), 1364, doi:10.1029/2003JA009984.

Liou K., P. T. Newell, C.-I. Meng, C.-C. Wu, and R. P. Lepping (2004), On the relationship between shock-induced polar magnetic bays and solar wind parameters, *J. Geophys. Res.*, *109*, A06306, doi:10.1029/2004JA010400.

Loomer, E. I., and J. C. Gupta (1980), Some characteristics of high-latitude substorms. *J. Atmos. Terr. Phys.*, *42*, 645–652.

Lyons, L. R., D. Y. Lee, C. P. Wang, and S. B. Mende (2005), Global auroral responses to abrupt solar wind changes: Dynamic pressure, substorm, and null events, *J. Geophys. Res.*, *110*, A08208, doi:10.1029/2005JA011089.

Meurant, M., J. C. Gerard, C. Blockx, V. Coumans, B. Hubert, M. Connors, L. R. Lyons, and E. Donovan (2005), Comparison of intense nightside shock-induced precipitation and substorm activity, *J. Geophys. Res.*, *110*, A07228, doi:10.1029/2004JA010916.

Miyashita, Y., K. Keika, K. Liou, S. Machida, Y. Kamide, Y. Miyoshi, Y. Matsumoto, I. Shinohara, Y. Saito, and T. Mukai (2010), Plasma sheet changes caused by sudden enhancements of the solar wind pressure, *J. Geophys. Res.*, *115*, A05214, doi:10.1029/2009JA014617.

Patel, V. L. (1968), Sudden impulses in the geomagnetotail, *J. Geophys. Res.*, *73*, 3407–3418, doi:10.1029/JA073i011p03407

Petrinec, S. M., and C. T. Russell (1996), Near-Earth magnetotail shape and size as determined from the magnetopause flaring angle, *J. Geophys. Res.*, *101*(A1), 137–152.

Runov, A., V. Angelopoulos, and X.-Z. Zhou (2012), Multipoint observations of dipolarization front formation by magnetotail reconnection, *J. Geophys. Res.*, *117*, A5, doi:10.1029/2011JA017361.

Schieldge, J. P., and G. L. Siscoe (1970), A correlation of the occurrence of simultaneous sudden magnetospheric compressions and geomagnetic onsets with selected geophysical indices, *J. Atmos. Terr. Phys.*, *32*, 1819.

Shi, Q.-Q., et al. (2012), THEMIS observations of ULF wave excitation in the nightside plasma sheet during sudden impulse events, *J. Geophys. Res. Space Physics*, *118*, 284–298, doi:10.1029/2012JA017984.

Shue, J. H., et al. (1998), Magnetopause location under extreme solar wind conditions, *J. Geophys. Res.*, *103*, 17,691–17,700, doi:10.1029/98JA01103.

Sitnov, M. I., M. Swisdak, and A. V. Divin (2009), Dipolarization fronts as a signature of transient reconnection in the magnetotail, *J. Geophys. Res.*, *114*, A04202, doi:10.1029/ 2008JA013980.

Sugiura, M., T. L. Skillman, B. G. Ledley, and J. P. Heppner (1968), Propagation of the sudden commencement of July 8, 1966, to the magnetotail, *J. Geophys. Res.*, *73*, 6699–6709, doi:10.1029/JA073i021p06699.

Takeuchi T., C. T. Russell, and T. Araki (2002), Effect of the orientation of interplanetary shock on the geomagnetic sudden commencement, *J. Geophy. Res.*, *107*(A12), 1423, doi:10.1029/2002JA009597.

Tsurutani, B. T., and X.-Y. Zhou (2003), Interplanetary shock triggering of substorms: WIND and POLAR, *Adv. Space Res.*, *31*(4), 1063–1067.

Tsyganenko, N. A. (1996), Effects of the solar wind conditions on the global magnetospheric configuration as deduced from data-based field models, in Proceedings of the Third International Conference on Substorms, Eur. Space Agency Spec. Publ. ESA SP-389, pp.181–186, Paris.

Zhou, X.-Y., 0. Russell, J. T. Gosling, and D. G. Mitchell (1997), Three spacecraft observations of the geomagnetic tail during moderately disturbed conditions: Structure and evolution of the current sheet, *J. Geophys. Res.*, *102*, 14,415–14,424.

Zhou, X.-Y., and B. T. Tsurutani (2001), Interplanetary shock triggering of nightside geomagnetic activity: Substorms, pseudobreakups, and quiescent events, *J. Geophys. Res.*, *106*, 18,957–18,967, doi:10.1029/2000JA003028.

Zhou, X.-Y., and B. T. Tsurutani (2002), Interplanetary shock effects on the nightside auroral zone, magnetosphere and ionosphere, in Proceedings of COSPAR Colloquium on Space Weather Study Using Multi-Point Techniques, edited by Ling-Hsiao Lyu, COSPAR Colloquia Series, 12, Elsevier Sci. Ltd., 139–147.

Zhou, X.-Z., et al. (2009), Ion distributions near the reconnection sites: Comparison between simulations and THEMIS Observations, *J. Geophys. Res.*, *114*, A12211, doi:10.1029/2009JA014614.

Zhou, X.-Z., Y. S. Ge, V. Angelopoulos, A. Runov, J. Liang, X. Xing (2012a), Dipolarization fronts and associated auroral activities: 2. Acceleration of ions and their subsequent behavior, *J. Geophys. Res.*, *117*, A10216, doi:10.1029/2012JA017677.

Zhou, X.-Z., V. Angelopoulos, A. Runov, J. Liu, and Y. S. Ge (2012b), Emergence of the active magnetotail plasma sheet boundary from transient, localized ion acceleration, *J. Geophys. Res.*, *117*, A10216, 9 p., doi:10.1029/2012JA018171.